Integrated physiological, transcriptomics, and metabolomics offer novel insights into the mechanisms of antimony resistance in Glycine max L

Liang You
Hunan University of Humanities, Science and Technology
Sha Gong
Hunan University of Humanities, Science and Technology
Guoxiang Jiang
Hunan University of Humanities, Science and Technology
Renyan Duan
Hunan University of Humanities, Science and Technology
Xincheng Wu
Hunan Agricultural University
Mingli Yan
Hunan Academy of Agricultural Sciences
Yuanwei Chen
Hunan Academy of Agricultural Sciences
Guohong Xiang
Hunan University of Humanities, Science and Technology
Yuhui Yuan
Hunan University of Humanities, Science and Technology
Junhe Hu
Hunan University of Humanities, Science and Technology
Yong Chen
Hunan University of Humanities, Science and Technology
Xianjun Liu
xjliu82@126.com

Hunan University of Humanities, Science and Technology

Research Article

Keywords: Glycine max L., Sb stress, Physiological analysis, Transcriptomics, Metabolomics

Posted Date: November 27th, 2025

DOI: https://doi.org/10.21203/rs.3.rs-8058106/v1

Additional Declarations: No competing interests reported.

Integrated physiological, transcriptomics, and metabolomics offer novel insights into the mechanisms of antimony resistance in *Glycine max* L.

Liang You[1,2,†], Sha Gong [1,†], Guoxiang Jiang[1], Renyan Duan[1,2], Xincheng Wu[3], Mingli Yan[4,5], Yuanwei Chen[4], Guohong Xiang[1,2], Yuhui Yuan[1], Junhe Hu[1], Yong Chen[1], Xianjun Liu[1,2,5,*]

Abstract: Antimony (Sb), a toxic metalloid with significant phytotoxicity and potential carcinogenicity, threatens agricultural safety due to its widespread use. Soybean (*Glycine max* L.), a globally important source of edible oil and protein, has been studied for heavy metal resistance, yet its specific responses to Sb stress remain unclear. Using integrated phenotypic, physiological, transcriptomic, and metabolomic analyses of Sb(III)-stressed soybean, we observed dose-dependent phytotoxicity, including leaf wilting, root damage, and biomass reduction. Despite these symptoms, soybean exhibited strong Sb tolerance, accumulation, and translocation capacity. Multi-omics analysis revealed dose-dependent coordinated upregulation of detoxification genes (e.g., *ABC transporters*, *CYPs*, and *HSP26-A*) and identified three key metabolic pathways contributing to Sb tolerance: (1) flavonoid biosynthesis, (2) alanine, aspartate, glutamate metabolism, and (3) isoquinoline alkaloid biosynthesis. Together, these components may constitute a coherent molecular defense network against Sb toxicity. Our findings provide novel insights into the mechanisms of Sb tolerance in soybean and support the development of resistant cultivars for cultivation in contaminated areas.

Keywords: *Glycine max* L., Sb stress, Physiological analysis, Transcriptomics, Metabolomics

Introduction

Escalating anthropogenic activities, such as mining, industrial emissions, agricultural practices, and urban wastewater treatment, have significantly exacerbated global heavy metal (HM) contamination, presenting critical public health challenges [1]. Antimony (Sb), a toxic metalloid, is designated as a priority pollutant by both the US Environmental Protection Agency (USEPA) and European Union (EU), with its compounds (e.g., Sb_2O_3) recognized as human carcinogens by the U.S. National Toxicology Program [2]. Current industrial Sb utilization primarily occurs through flame retardants in various products, including plastics, coatings, electronics, and other items, which account for the majority of global Sb consumption [2-4]. The industrial -driven demand for Sb has intensified mining activities, with unregulated mining, weathering of sulfide ores, and other anthropogenic activities facilitating Sb dispersion into soils and aquatic environments [5], thereby significantly compromising the essential environmental conditions for plant survival and growth.

Sb is recognized as a potent environmental toxin, predominantly existing in the forms of Sb(III) and Sb(V) [6]. To elucidate Sb phytotoxicity, recent multiple investigations have systematically characterized Sb stress responses across diverse plant species. Sb-induced phytotoxicity primarily involves the Sb migrate from soil to roots, followed by its transport through cell walls or xylem vessels, facilitating systemic distribution within the plant [7, 8]. Exposure of Acorus calamus to Sb(III) and Sb(V)

elicited concentration-specific growth responses: low concentrations maintained or marginally stimulated growth, while high concentrations significantly inhibited growth by reducing photosynthetic pigments, impairing photosynthesis, and decreasing biomass [9]. In *Oryza sativa* L., Sb(III) showed higher phytotoxicity than Sb(V), with metabolomic studies revealing Sb-induced metabolic shifts, including increased glycosyl flux into oligosaccharide biosynthesis, potentially facilitating reactive oxygen species (ROS) scavenging, cell wall strengthening, and membrane permeability regulation [10]. Another study found that both Sb forms consistently triggered oxidative stress, activating superoxide dismutase (SOD) and ascorbate peroxidase (APX) [11]. Furthermore, Sb accumulation impairs plant physiology by disrupting nutrient uptake, inducing lipid peroxidation, altering hormone balance, and causing structural changes, ultimately affecting growth and development [12]. In summary, while extensive physiological studies on plant responses to Sb stress have been conducted, elucidating the underlying molecular mechanisms remains critical and has garnered significant research attention.

Advances in sequencing technologies and reduced costs have established transcriptomics and metabolomics as essential tools for uncovering the molecular mechanisms underlying plant responses to Sb stress and identifying key regulatory genes in species, such as *Arabidopsis thaliana* [8], *Oryza sativa* L. [10, 13], *Festuca arundinacea* [14], and *Boehmeria nivea* L. [15]. Transcriptomic analysis of *A. thaliana* under Sb stress highlighted the upregulation of glutathione-related genes (*GSTF6*, *GSTU7*, *GSTU8*) and ABC transporters (*ABCB15*, *ABCC1*, *ABCC2*), indicating their pivotal roles in Sb uptake and detoxification [8]. Metabolomic analysis revealed significant up-regulation of oligosaccharides (sucrose, stachyose, and 1-kestose) in rice under Sb stress, indicating their involvement in antioxidant and cell wall biosynthesis [10]. Meanwhile, selenium (Se) has been proposed to alleviate Sb toxicity in rice, potentially by enhancing starch, sucrose, and fructose levels and up-regulating genes associated with chlorophyll, carotenoid, glucose, and sucrose synthesis [13]. Additionally, under Sb stress, pathways related to catalytic activity, carbohydrate metabolism, phenylpropanoid biosynthesis, cell wall modification [15], and glycine, serine, and threonine metabolism [14] are activated, with genes in these pathways contributing to Sb detoxification. While these findings provide a foundation for understanding the molecular mechanisms of plant responses to Sb, further identification of Sb-responsive genes and metabolites across different species is essential to fully elucidate these mechanisms.

Soybean (*Glycine max* L.), a global crucial source of edible oil and protein, contains significant amounts of fats, carbohydrates, vitamin C and minerals [16]. Rising living standards are driving increasing demands for enhanced soybean yield and quality. Regions with high-Sb background levels, exemplified by the Xikuangshan mining areas, exhibit environmental Sb contaminations (soil: 101-5,045 $mg \cdot kg^{-1}$; water: 17-288 $\mu g \cdot L^{-1}$) that exceeds the WHO-recommended thresholds (soil: 36 $mg \cdot kg^{-1}$; water: 0.02 $\mu g \cdot L^{-1}$) [2]. These Sb-contaminated areas severely impair crop productivity through Sb-induced phytotoxicity and posing substantial health risks to local residents, rendering the development of Sb-resistant cultivars an urgent agricultural priority. However, the molecular mechanisms underlying soybean responses to Sb stress remain poorly characterized. Elucidating these pathways and functionally characterizing the associated stress-responsive genes are critical for optimizing soybean agronomic traits and accelerating molecular breeding in Sb-polluted mining ecosystems.

To investigate the mechanisms underlying soybean's response to Sb, integrated physiological, transcriptomic, metabolomic profiling are employed in this study. Specific objectives included: (a) assessing growth, Sb accumulation, and Sb transport in soybean seedlings at varying Sb concentrations; (b) identifying differentially expressed genes (DEGs) and differentially accumulated metabolites (DAMs) along with their key pathway; (c) elucidating the molecular mechanisms driving transcripts and metabolite changes under Sb stress. This research lays a foundation for future studies and offers new insights into plant-based remediation strategies.

Materials and Methods

Plant materials, growth conditions, and treatment

The commercial soybean cultivar 'Zhonghuang 13', provided by the Crop Research Institute of the Hunan Academy of Agricultural Sciences, was used in this study. Seeds were sown in conical plastic pots (10 cm × 10 cm × 10 cm), with a total of 20 pots each containing three plants. Plants were cultivated in a greenhouse under a 14 h/10 h light/dark cycle at 24°C/20°C. The growth substrate consisted of a moistened mixture containing 1/2 white vermiculite, with approximately 5 kg added per pot. To ensure optimal soil porosity, irrigation was performed by immersing the base trays. Approximately 30 days after sowing, when the main stem had developed five compound leaves, plants were divided into control and Sb treatment groups, each with 5 replicates, while soil moisture was maintained at 50±5%. To evaluate soybean seedling responses to varying Sb concentrations (low, medium, high), 1 L solutions of potassium antimonyl tartrate ($KSbC_4H_4O_7 \cdot 0.5H_2O$, Sb(III)) at concentrations of 0, 1, 10, and 50 $mmol \cdot L^{-1}$ were slowly applied to the root zone of the respective treatment groups, with supplemental irrigation every three days. These treatments were designated as Sb0, Sb1, Sb10, and Sb50, respectively. Plant phenotypes were monitored daily following Sb exposure, and the time point at which significant morphological changes became evident was selected for subsequent analysis. At this stage, root tissues from all treatment groups were collected and stored at –80°C for physiological, transcriptomic, and metabolomic assays. Fresh leaf samples were also harvested for chlorophyll quantification, while root-adjacent soil and the remaining plant material were collected for the determination of Sb accumulation.

Determination of Sb accumulation and physiological index

Sb accumulation in plants and soil

To evaluate the enrichment and translocation factors of Sb in soybean organs, roots, stems, leaves, and whole plants from both control and Sb-treated groups were dried. Samples were initially placed in an oven at 105°C for 0.5 h, then further dried at 75°C until a constant weight was achieved. Afterward, the samples were ground into powder for digestion. Air-dried soil samples were sieved through a 2 mm mesh and ground into powder. Next, 0.3 g of plant or soil sample was weighed into a digestion tube, moistened with deionized water, and digested in an automatic digestion system (ADB-50, Beijing LabTech, China) using 5 mL hydrochloric acid (ρ = 1.19 g/mL), 9 mL nitric acid (ρ = 1.19 g/mL), and 5 mL hydrofluoric acid (ρ = 1.16 g/mL) at 120 °C for 3 h. After digestion, the mixture was diluted with 2% nitric acid to a final volume of 25 mL, shaken thoroughly, and allowed to settle. The supernatant was analyzed for Sb content using inductively coupled plasma mass spectrometry (ICP-MS, PerkinElmer NexION® 2000,

USA). The bioconcentration factors (BCFs, Sb in whole plant/Sb in soil) and translocation factors were calculated: TF_{RS} (Sb in stem/Sb in root), TF_{SL} (Sb in leaf/Sb in stem), and TF_{RL} (Sb in leaf/Sb in root).

Physiological index

To investigatethe physiological response of soybean to Sb stress, antioxidant enzyme activities in roots and chlorophyll content in leaves were measured using commercial assay kits (Beijing Boxbio Science & Technology Co., Ltd.). The following kits were used: Catalase (CAT, AKAO003-1M), Superoxide Dismutase (SOD, AKAO001M-100S), Peroxidase (POD, AKAO005M), Malondialdehyde (MDA, AKFA013M), Reduced Glutathione (GSH, AKPR008M), and Plant Chlorophyll (AKPL003M). All procedures were performed strictly according to the manufacturer's instructions, with each physiological parameter measured in at least three biological replicates.

RNA extraction and transcriptome analysis

To explore the molecular basis of soybean response to different Sb concentrations, high-throughput RNA sequencing was performed using the Illumina platform. Total RNA was extracted from soybean roots under four Sb treatments using the TRIzol method, with three biological replicates per treatment. cDNA libraries were prepared according to Fan et al. [14], followed by sequencing on the Illumina NovaSeq X Plus instrument by Gene Denovo Biotechnology Co., Ltd. (Guangzhou, China).

Raw reads were subjected to quality control using fastp to obtain clean reads. Ribosomal RNA was then removed using Bowtie2, and the filtered reads were aligned to the soybean reference genome (https://ngdc.cncb.ac.cn/, Accession: GWHBWDJ00000000.1) using HISAT2. Transcript assembly was performed based on the HISAT2 alignment results using StringTie software, and gene expression levels were quantified for each sample with RSEM. Expression values were reported as fragments per kilobase of transcript per million mapped reads (FPKM). Subsequent analyses included DEGs enrichment, expression trend analysis, and Weighted gene co-expression network analysis (WGCNA) analysis. These bioinformatic analyses were carried out using Omicsmart (http://www.omicsmart.com), a real-time interactive online platform for data analysis.

Metabolomic analysis

To comprehensively profile the metabolites produced by soybean under different Sb concentrations and compare metabolic differences across the four treatments (with three biological replicates each), a quantitative metabolomic analysis was performed using LC-MS/MS on 12 soybean root samples corresponding to those used in the transcriptomic study. Sample preparation and metabolomic analyses were conducted by Gene Denovo Biotechnology Co., Ltd. (Guangzhou, China)..

LC-MS/MS analyses were performed using a Vanquish UHPLC system (ThermoFisher, Germany) coupled with an Orbitrap Q Exactive™ HF-X mass spectrometer (ThermoFisher, Germany). Both positive ion mode (POS) and negative ion mode (NEG) were utilized for ionization. Following raw mass spectrometry data acquisition, data processing steps including file conversion, peak identification, filtering, data alignment, normalization of quantification results, and quality control, were performed according to the method of Xu et al. [17]. OPLS-DA was conducted using the R package (ropls), and differential metabolites were identified by applying thresholds for *p*-values and variable importance on projection (VIP).

Quantitative real-time PCR (qRT-PCR) and statistical analysis

To validate the RNA-Seq results, nine significantly DEGs were selected for qRT-PCR analysis. The procedures for RNA extraction, reverse transcription, and qRT-PCR followed the method described by You et al. [18]. GmActin [19] was used as the reference gene for normalization. Gene expression was quantified using a CFX96 real-time system (BIO-RAD, USA), and relative expression levels were calculated using the $2^{-\Delta\Delta Ct}$ method. Three biological replicates and three technical replicates were performed for each gene and sample.

Statistical analyses were conducted to evaluate significant differences in physiological indices, gene expression, and metabolite abundance across different Sb treatments, using one-way ANOVA and Tukey's correction. Results were visualized with GraphPad Prism software (version 8.2.1), and significant differences ($p < 0.05$) are indicated by different lowercase letters.

Results

Phenotypic and Sb accumulation characteristics of soybean under Sb stress

To investigate the tolerance, absorption, and transport mechanisms of soybean seedlings under Sb stress, the seedlings were treated with four Sb concentrations: 0 (Sb0), 1 (Sb1), 10 (Sb10), and 50 (Sb50) mmol·L^{-1}. Soil Sb content in the root zone increased with treatment concentration, averaging 0.6, 10.8, 90.0, and 424.0 mg/kg under Sb0, Sb1, Sb10, and Sb50, respectively (Table S1), respectively. No significant morphological changes were observed initially; however, after 5 days, severe wilting and chlorosis developed in the lower leaves of Sb50-treated plants (Fig. 1A). Evans Blue staining revealed dark blue coloration in root tissues under Sb10 and Sb50 treatments (Fig. 1B), indicating loss of membrane integrity. While root dry weight remained unaffected across treatments (Fig. 1C), low Sb concentrations stimulated stem growth (Fig. 1D), whereas high concentrations significantly inhibited biomass in stems and leaves (Fig. 1E). These findings indicate a dose-dependent response of soybean seedlings to Sb stress: low levels promote stem growth, while high levels induce phytotoxicity, manifested as leaf scorch, wilting, biomass reduction, and root membrane damage.

Based on the phenotypic results of soybean seedlings after 5 days of Sb treatment, we further evaluated Sb uptake and translocation. Under Sb1 treatment, stems exhibited the highest Sb accumulation, likely related to increased biomass, whereas Sb10 treatment resulted in a decreasing Sb gradient from roots to leaves. Tissues in the Sb50 group consistently accumulated Sb exceeding soil concentrations, with bioaccumulation factors (BCFs) >1 across all Sb-treated groups (Table S1). Transfer factors (TFs) differed significantly among treatments (Table S2): the root-to-stem TF under Sb1 was the highest (1.65), while Sb50 yielded TFs of 0.91 (root-to-stem), 1.22 (stem-to-leaf), and 1.12 (root-to-leaf). In contrast, all TFs in the Sb10 treatment were below 0.64, with a particularly low TF (root-to-leaf) of only 0.40. Strong positive correlations (r = 0.982-0.999) were observed between tissue and soil Sb concentrations (Table S3). Overall, soybean seedlings demonstrated strong Sb accumulation and tolerance, with tissue-specific Sb enrichment increasing in proportion to soil Sb levels. Elevated Sb exposure also enhanced inter-tissue translocation efficiency, characterized by stable TFs and Sb partitioning from roots to aerial organs via passive diffusion.

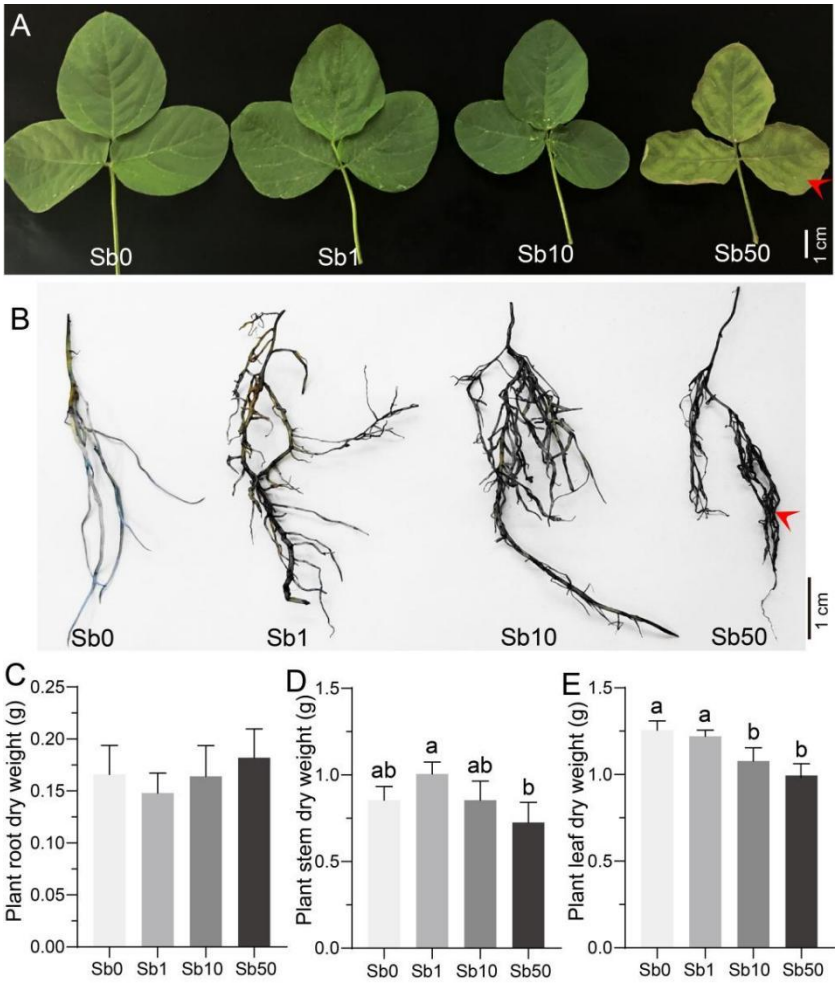

Figure 1. Effect of different Sb concentrations on soybean phenotypic characteristic. **A** Morphological changes in soybean leaves under different Sb concentrations. **B** Sb-treated soybean root tissues stained with Evans Blue. Red arrows indicate the distinct morphological alterations in soybean tissues induced by Sb exposure. Bar: 1 cm. **C-E** Dry weight of root (C), stem (D), and leaf (E) tissues in soybean under different Sb treatments. Sb0, Sb1, Sb10, and Sb50 represent treatments with 0, 1, 10, and 50 mol·L^{-1} Sb aqueous solutions, respectively. Different lowercase letters represent significant differences at $p < 0.05$ level using one-way ANOVA and Tukey's correction (Mean ± SE, n = 6).

Physiological changes of soybean under Sb stress

To further investigate the physiological effects of Sb accumulation in soybean seedlings, key physiological indicators, including CAT, SOD, POD, MDA, and GSH in roots, as well as chlorophyll content in leaves. Results demonstrated that compared to the control, CAT activity was significantly enhanced across Sb treatments, increasing by 58.2% under Sb50 (Fig. 2A). Root SOD activity and GSH content decreased under low Sb concentrations (Sb1 and Sb10) but rose markedly under Sb50 by 84.7% and 30.4%, respectively (Fig. 2B, 2E), indicating that elevated Sb levels disrupt cellular homeostasis and activate antioxidant defense mechanisms. Conversely, POD activity gradually declined as Sb concentration increased (Fig. 2C). MDA, a key indicator of membrane lipid peroxidation [14], was significantly elevated in root tissues across all Sb treatments (Fig. 2D). Chlorophyll content in leaves decreased most substantially under Sb50 (Fig. 2F), consistent with the observed leaf scorching symptoms. Together, these results indicate that Sb triggers dose-dependent physiological changes in

soybean seedlings: low concentrations elicit early adaptive reactions, while high concentrations induce oxidative stress and activate antioxidant defenses.

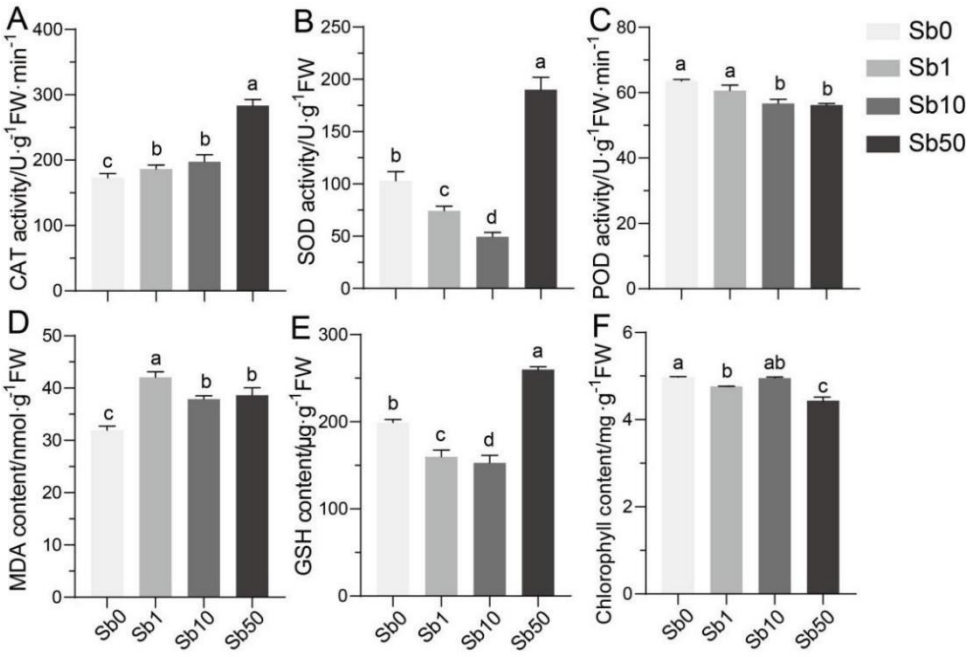

Figure 2. Effect of different Sb stress on soybean physiological parameters. **A-C** Changes in CAT (A), SOD (B), and POD (C) activity in soybean seedling root tissues under different Sb stress. **D-E** Changes in MDA (D) and GSH (E) content. **F** Changes in total chlorophyll content in soybean seedling leaf tissues. Different lowercase letters represent significant differences at $p < 0.05$ level using one-way ANOVA and Tukey' s correction (Mean ± SE, n = 6).

Transcriptome analysis

Transcriptome sequencing and DEGs identification

RNA-seq analysis of soybean roots under Sb0, Sb1, Sb10, and Sb50 treatments (with three biological replicates per group) produced an average of 42.2, 40.6, 40.8, and 40.7 million raw reads per sample, respectively (Table S4). After stringent quality control, over 99.97% of high-quality clean reads were retained in each group. These reads were aligned to the *Glycine max* L. reference genome 'Zhonghuang 13', achieving a mapping rate exceeding 93.12% for all samples (Table S4).

Using a threshold of *P*-value < 0.05 and $|\log_2(\text{fold change})| > 1$, we identified DEGs in each comparison: Sb0-vs-Sb1 (1,044), Sb0-vs-Sb10 (1,500), Sb0-vs-Sb50 (3,427), Sb1-vs-Sb10 (618), Sb1-vs-Sb50 (4,778), and Sb10-vs-Sb50 (3,150) (Fig. 3A). Notably, Sb1 treatment resulted in 2.88-fold more down-regulated than up-regulated DEGs relative to Sb0, whereas Sb10 treatment compared to Sb1 showed predominantly up-regulated DEGs. Other pairwise comparisons maintained relatively stable DEG numbers. These patterns suggest a dose-dependent transcriptional response: low-concentration Sb1 stress mainly suppresses gene expression, while moderate Sb10 exposure activates transcriptional up-regulation. Additionally, venn diagram analysis of DEGs from the Sb0-vs-Sb1, Sb0-vs-Sb10, and Sb0-vs-Sb50 comparisons revealed 297 core DEGs shared across Sb treatments (Fig. S1A, Table S5), with the majority (246/297) being downregulated (Fig. S1B). This predominant downregulation directly corresponds to the expression pattern observed in the Sb0-vs-Sb1 comparison, implicating their potential role in the soybean Sb stress response through suppressed expression.

Gene ontology (GO) and Kyoto encyclopedia of genes and genomes (KEGG) pathway analysis

To elucidate the functional roles of differentially expressed genes (DEGs) in soybean's response to Sb stress, we performed GO and KEGG enrichment analyses on DEG sets from different comparative groups. GO analysis showed that 23 of the top 27 significantly enriched terms across the six comparisons were related to carbohydrate biosynthesis (6 terms), transmembrane transport (8 terms), cell wall organization (2 terms), antioxidant activity (5 terms), and metal ion binding (2 terms) (Fig. 3B, Table S6). Analysis of the 297 core DEGs further highlighted significant enrichment in peroxidase activity, response to oxidative stress, and transmembrane transporter activity (Fig. S1C). These results indicate that Sb stress markedly affects carbohydrate metabolism and antioxidant-related processes in soybean roots, while also influencing cell membrane integrity and metal ion binding capacity.

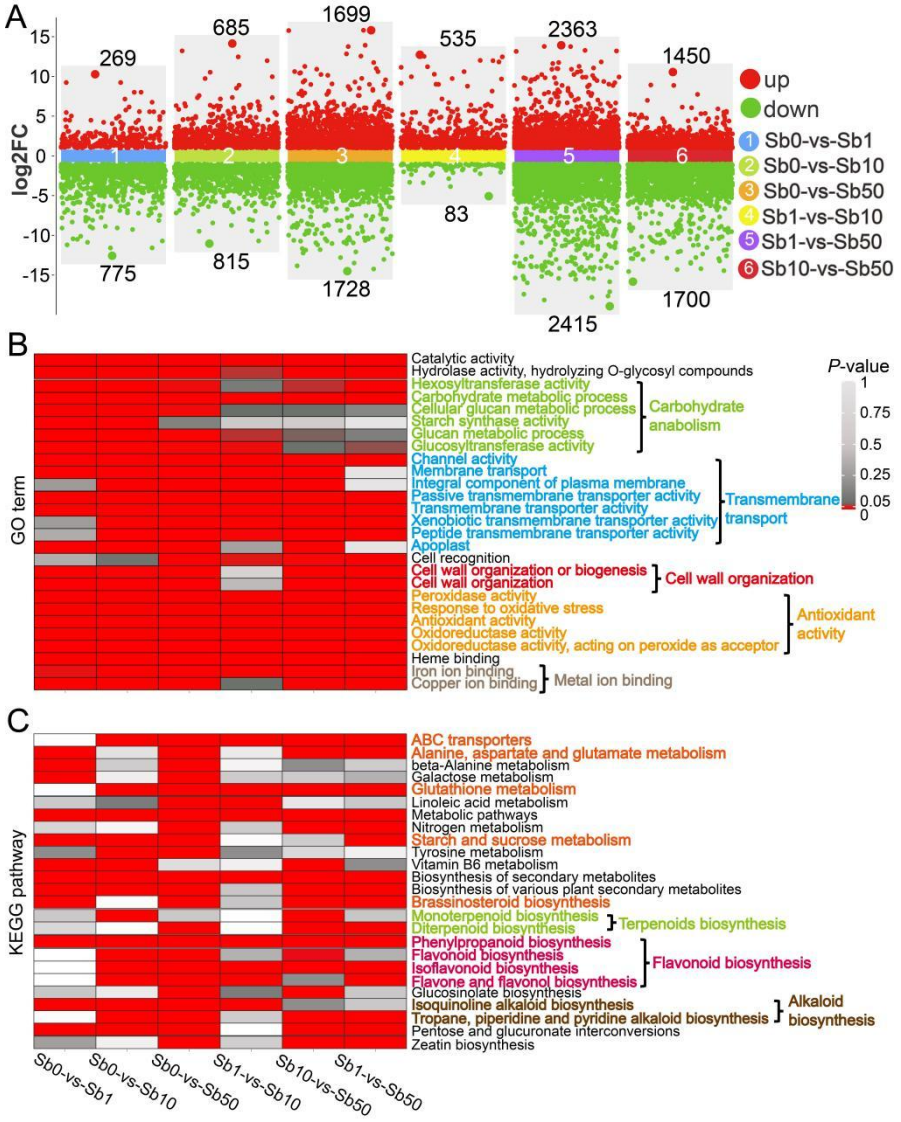

Figure 3. Analysis of DEGs related to Sb stress response in soybean. **A** Scatterplot analysis of DEGs between different Sb treatments. **B** Differential GO enrichment heat map between Sb treatments. **C** KEGG enrichment heat map of different Sb treatments. Heat map red modules indicate significant differences with *P*-values of less than 0.05. Key GO terms and KEGG pathways are marked in colored font.

KEGG pathway analysis revealed significant enrichment ($P < 0.05$) in 23 metabolic pathways, with 13 showing consistent enrichment across comparisons. These included ABC transporters (ko02010),

alanine, aspartate and glutamate metabolism (ko00250), glutathione metabolism (ko00480), starch and sucrose metabolism (ko00500), terpenoid biosynthesis (ko00904, ko00902), flavonoid metabolism (ko00940, ko00941, ko00943, ko00944), and alkaloid biosynthesis (ko00950, ko00960) (Fig. 3C, Table S7). These pathways were also enriched among the common DEGs from the Sb0-vs-Sb1, Sb0-vs-Sb10, and Sb0-vs-Sb50 comparisons (Fig. S1D). The enrichment results highlight key metabolic adaptations to Sb stress, including flavonoid-mediated detoxification, glutathione and ABC transporter-assisted chelation/transport, and terpenoid/alkaloid -based defense mechanisms. Together, these findings outline a systemic metabolic framework underlying Sb tolerance, offering potential targets for breeding Sb-resistant crops through metabolic engineering.

Expression profiling and functional characterization of DEGs

To elucidate the expression dynamics and functional roles of regulatory genes in soybean roots under Sb stress, we performed trend analysis on 4,429 DEGs from the Sb0-vs-Sb1, Sb0-vs-Sb10, and Sb0-vs-Sb50 comparisons. Most DEGs were predominantly clustered into four expression modules: bright green (Fig. S2A, Profile 12 and 19), purple (Fig. S2B, Profile 2), orange (Fig. S2C, Profile 0 and 9), and green (Fig. S2D, Profile 3).

The bright green module was significantly enriched in GO terms related to oxidoreductase activity, peroxidase activity, iron ion binding, and oxidative stress response (Table S8). Notably, it contained 18 *ABC transporter* genes, 34 *cytochrome P450* (*CYP*) genes, 9 *HSP26-A* (*GSTU23*) genes, and 7 *peroxidase* genes that were markedly upregulated under Sb exposure, suggesting their key involvement in Sb^{3+} transport and detoxification (Table S9). In contrast, genes in the purple module were initially downregulated under low Sb stress but stabilized thereafter (Fig. S2B). These genes were functionally enriched in peroxidase activity and oxidative stress response, yet were primarily associated with carbohydrate metabolism and transport (Table S8), implying that suppression of carbohydrate synthesis-related genes contributes to Sb tolerance. Genes in the orange module, largely related to transmembrane transport, were significantly downregulated (677 of 1,041 genes; Fig. S2C) under high Sb stress, indicating Sb-induced inhibition of cellular transport processes. Finally, genes in the green module displayed a down-then-up expression pattern and were enriched in copper ion binding, membrane transport, and cell wall organization and modification (Fig. S2D; Table S8).

WGCNA analysis of the DEGs

To identify gene co-expression modules associated with Sb tolerance and uncover hub genes responsive to Sb stress in soybean, we performed WGCNA using 4,429 DEGs identified between Sb-treated (Sb1, Sb10, Sb50) and control (Sb0) groups. The analysis organized the DEGs into 13 distinct co-expression modules (Fig. 4A). A heatmap depicting module membership (MM) correlations with physiological traits—including soil Sb (Soil_Sb), root Sb (Root_Sb), root dry weight (Root_dry), MDA, SOD, GSH, CAT, and POD, showed that the pink, blue, and green modules were strongly positively correlated with Root_Sb, root dry weight, and CAT activity, but negatively correlated with POD activity (Fig. 4B). These three modules also showed strong inter-module correlations ($r > 0.82$; Fig. 4C). GO enrichment analysis indicated their involvement in oxidoreductase activity, iron ion binding, peroxidase activity, and transmembrane transport (Fig. S3A). KEGG analysis further revealed significant enrichment in

glutathione metabolism, alanine-aspartate-glutamate metabolism, isoquinoline alkaloid biosynthesis, ABC transporters, and flavonoid biosynthesis (Fig. S3B). Using Cytoscape, we identified the top 10 hub genes (highest MM) in the pink (Fig. 4D), blue (Fig. 4E), and green (Fig. 4F) modules. Notable hub genes included *respiratory burst oxidase homolog protein C-like* (*RBOHC*), *chalcone isomerase 4* (*CHI4*), *peroxidase 52* (*PER52*), and *probable glutathione S-transferase* (*HSP26-A*), suggesting their key roles in mediating soybean's response to Sb stress.

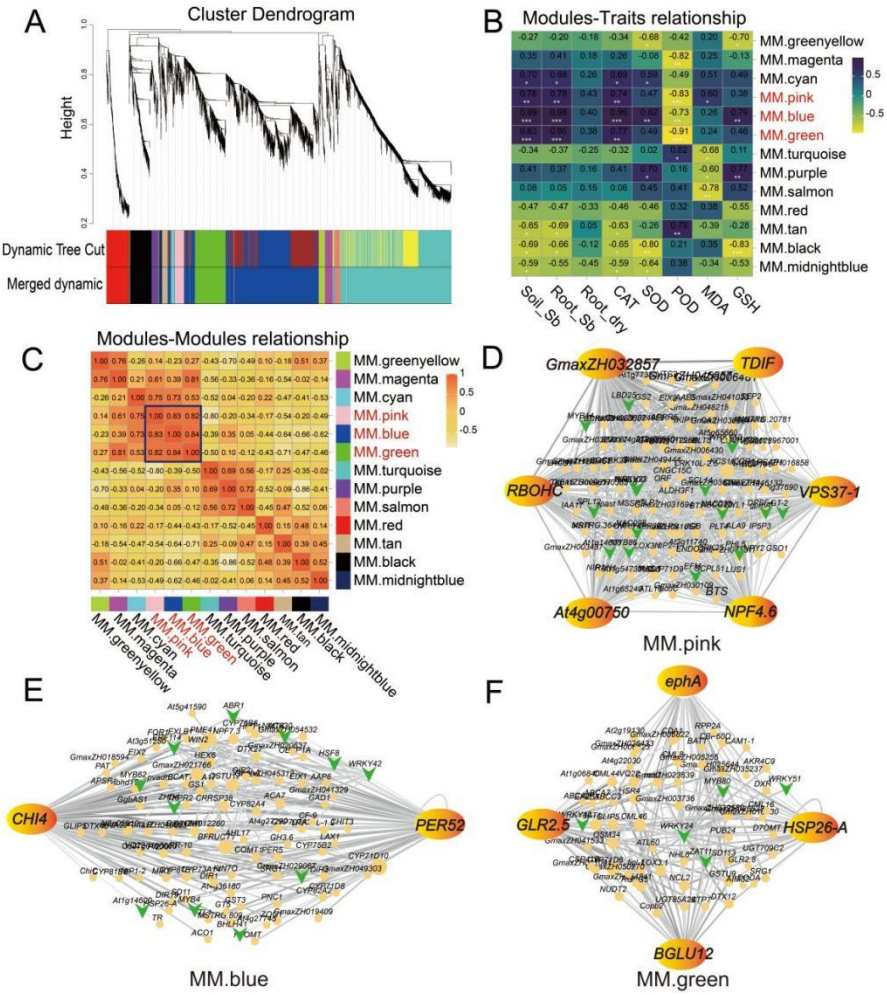

Figure 4. Analysis of DEGs related to Sb stress response in soybean. **A** Scatterplot analysis of DEGs between different Sb treatments. **B** Differential GO enrichment heat map between Sb treatments. **C** KEGG enrichment heat map of different Sb treatments. D-F Hub gene analysis of the pink (D), blue (E) and green (F) modules. Heat map red modules indicate significant differences with *P*-values of less than 0.05. Key GO terms and KEGG pathways are marked in colored font.

Metabolomic analysis of soybean roots under Sb stress

This study utilized LC-MS/MS-based untargeted metabolomics to identify metabolites responsive to Sb stress in soybean. A total of 2,971 metabolites were detected in mixed positive/negative ion mode (1,549 in positive mode, 1,422 in negative mode). Orthogonal partial least squares discriminant analysis (OPLS-DA) analysis implemented with the R package ropls showed clear separation between each treatment group (Sb1, Sb10, Sb50) and the control (Sb0), indicating substantial metabolic reprogramming under Sb stress (Fig. S4A).

Using thresholds of VIP > 1, $P < 0.05$, and |Fold change| > 1.5, DAMs were identified. These were primarily classified as Phenylpropanoids and polyketides (57 metabolites), Lipids and lipid-like molecules (48), Organoheterocyclic compounds (47), and seven other major Superclasses (Fig. S4B. Pairwise comparisons identified 161 (75 up, 86 down), 93 (38 up, 55 down), and 476 (263 up, 213 down) DAMs in Sb0-vs-Sb1 (Fig. 5A), Sb0-vs-Sb10 (Fig. 5B), and Sb0-vs-Sb50 (Fig. 5C), respectively. KEGG enrichment analysis of the 647 DAMs revealed significant involvement in flavonoid metabolism (ko00941, ko00943, ko00944), alkaloid metabolism (ko00950, ko00996), alanine, aspartate and glutamate metabolism (ko00250), and ABC transporters (ko02010). Notably, 11, 10, 5, and 3 DAMs were specifically associated with ABC transporters, flavonoid biosynthesis, isoquinoline alkaloid biosynthesis, and alanine-aspartate-glutamate metabolism, respectively (Fig. 5D; Table S10), highlighting their potential importance in the Sb stress response.

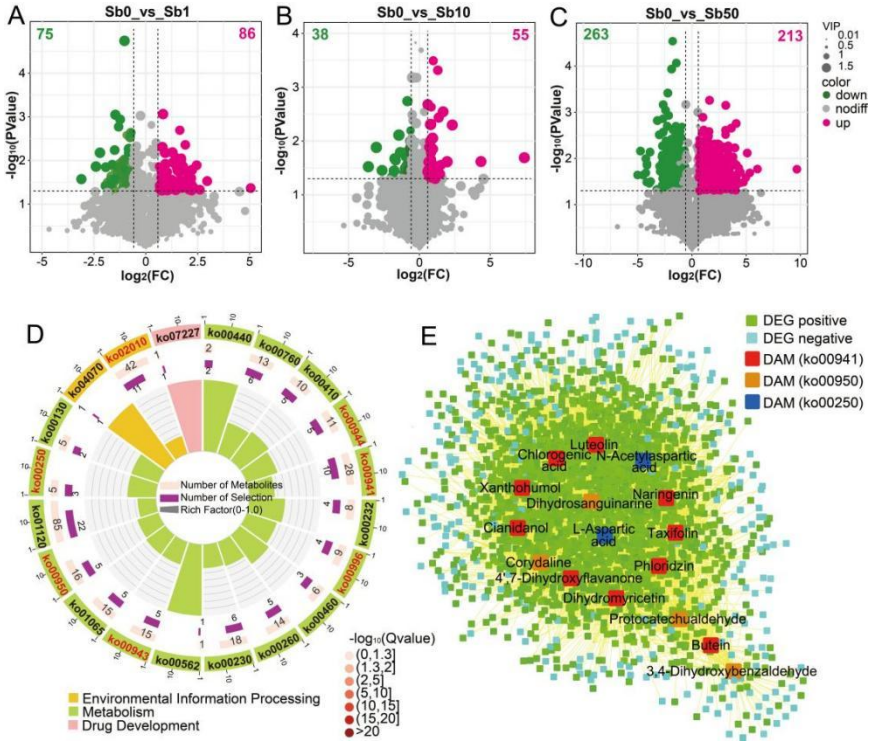

Figure 5. Metabolomic analysis in Soybean under Sb stress. **A-C** Volcano plot analysis of DAMs in Sb0-vs-Sb1 (A), Sb0-vs-Sb10 (B), and Sb0-vs-Sb50 (C) comparison groups. **D** Top 20 enriched KEGG pathways of all DAMs. **E** Correlation network analysis of DAMs and DEGs from metabolomic and transcriptomic data in representative KEGG pathways. Green and light blue squares denote up- and down-regulated DEGs, respectively, while red, orange, and blue squares represent DAMs in the ko00941, ko00950, and ko00250 pathways, respectively.

Combined transcriptomic and metabolomic analysis

Nine-quadrant plot and correlation network analysis of DAMs and DEGs

To explore transcriptomic-metabolomic associations, we analyzed 4,429 DEGs and 647 DAMs from the Sb0-vs-Sb1, Sb0-vs-Sb10, and Sb0-vs-Sb50 comparisons using a nine-quadrant plot (Fig. S5). DAMs and DEGs located in quadrants 3 and 7 showed positive correlations, whereas those in quadrants 1 and 9 displayed negative correlations. The number of DEGs and DAMs increased substantially in the Sb0-vs-Sb50 comparison (Fig. S5C) relative to Sb0-vs-Sb1 (Fig. S5A) and Sb0-vs-Sb10 (Fig. S5B), indicating a dose-dependent intensification of the molecular response under high Sb stress. To identify

key pathways involved, we constructed correlation networks between DAMs and DEGs associated with flavonoid biosynthesis (ko00941), isoquinoline alkaloid biosynthesis (ko00950), and alanine, aspartate, and glutamate metabolism (ko00250) across Sb concentrations (Fig. 5D). Notably, DAM–DEG correlations were predominantly positive, with most interactions being strong, suggesting that these metabolites play critical roles in regulating detoxification pathways under Sb toxicity.

Combined analysis of DAMs and DEGs in representative pathways

Flavonoid biosynthesis pathway

Flavonoids, a class of antioxidant secondary metabolites, help alleviate HMs toxicity in plants by scavenging ROS and inhibiting its generation [20]. Under Sb stress, we observed significant enrichment of both DEGs and DAMs related to flavonoid biosynthesis. Integrated transcriptomic and metabolomic profiling revealed systematic changes in the flavonoid pathway, marked by the up-regulation of metabolites such as isoliquiritigenin, butein, liquiritigenin, and naringenin chalcone across Sb treatments, while naringenin and phlorizin were down-regulated under high Sb50 exposure. Key biosynthetic genes, including *phenylalanine ammonia-lyase* (*PAL*), 4-*coumarate: CoA ligase* (*4CL*), c*halcone and stilbene synthase* (*CHS*), and *chalcone isomerase* (*CHI*), were consistently up-regulated (Table S11). Activation or up-regulation was also observed in isoflavonoid biosynthesis and flavone/flavonol biosynthesis pathways (Fig. 6A). These findings indicate that the coordinated up-regulation of DAMs and DEGs in flavonoid biosynthesis likely contributes to soybean's detoxification response against Sb-induced oxidative stress.

Alanine, aspartate, and glutamate metabolism pathway

Numerous studies have reported the enrichment of alanine, aspartate, and glutamate metabolism pathways in plants exposed to abiotic stresses such as cadmium (Cd) [21], lead (Pb) [22], and salt [23], suggesting their potential role in stress tolerance and detoxification. In this study, multiple DAMs and DEGs were enriched in these metabolic pathways. Key metabolites, including L-aspartate, L-asparagine, L-glutamate, 4-aminobutanoate, and L-glutamine, accumulated under Sb stress, particularly under high-concentration Sb50 treatment (Fig. 6B). Related pathways such as histidine metabolism, glutathione metabolism, purine metabolism, and arginine biosynthesis also exhibited alterations in metabolite abundance and gene expression. Notably, the expression patterns of DEGs involved in metabolic regulation did not fully align with changes in DAMs. Key genes including *aspartate carbamoyltransferase 1* (*PYRB1*), *asparagine synthetase 1/2* (*AS1/2*), and *glutamine synthetase 2* (*GS2*) were significantly downregulated under Sb stress, while five *glutamate decarboxylase 1* (*GAD1*) genes showed divergent expression trends (Table S11). In summary, this study highlights convergent changes in aspartate and glutamate metabolism in response to Sb stress, with related metabolites showing increased accumulation. However, the regulatory mechanisms underlying the discordant expression of DEGs and their functional roles in metabolic networks require further investigation.

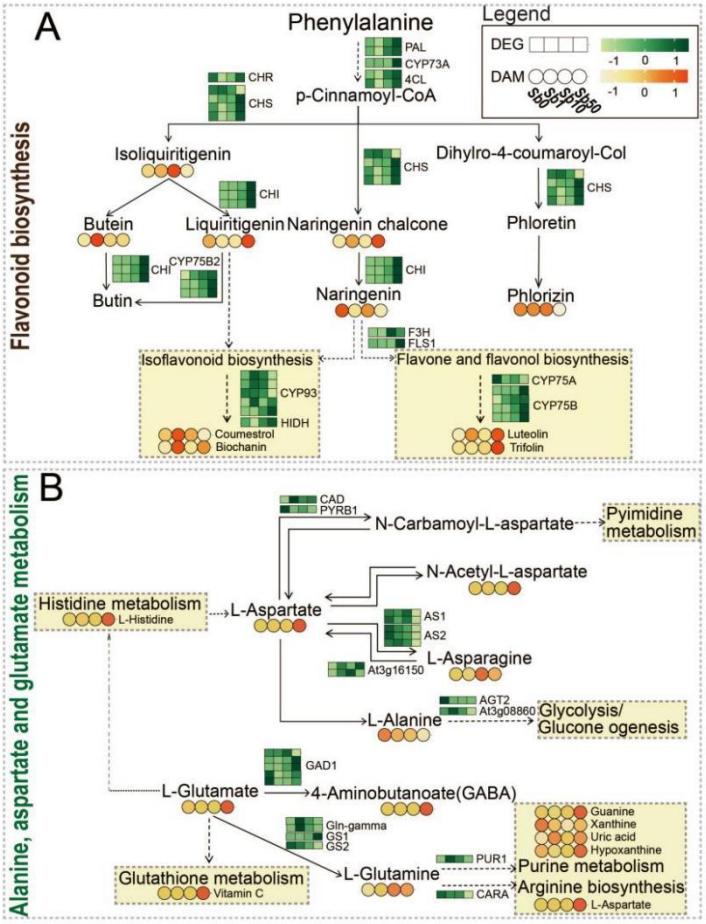

Figure 6. Regulatory network analysis of flavonoid biosynthesis (A) and alanine, aspartate, and glutamate metabolism (B) pathways. Squares represent DEGs, with darker green indicating higher gene expression levels. Circles represent DAMs, with darker orange indicating higher metabolite abundance. Solid arrows and dashed arrows were used to indicate direct and indirect molecular interactions, respectively. KEGG pathways schematic derived from https://www.kegg.jp/.

Isoquinoline alkaloid biosynthesis pathway

Alkaloids, recognized as pharmacologically essential constituents of traditional Chinese medicine, demonstrate potent antitumor efficacy against various cancers, including breast and colon malignancies [24]. Interestingly, alkaloid metabolism is also consistently implicated in plant adaptive responses to HMs stress [25]. Through integrated transcriptomic and metabolomic analysis and KEGG enrichment, we identified alkaloid biosynthesis as a significantly enriched pathway under Sb stress. Focusing on the co-enriched isoquinoline alkaloid biosynthesis pathway, we systematically characterized its regulatory network involving DEGs and DAMs. Network analysis indicated that phenylalanine, tyrosine, and tryptophan biosynthesis serve as upstream pathways for isoquinoline alkaloid production. Under Sb stress, several key genes were significantly upregulated, including two polyphenol oxidase (PPO) genes, four *asparagine synthetase 1* (*AS1*) genes, a *tyrosine aminotransferase* (*TAT*), and an *NAD-dependent malic enzyme* (*maol*). Additionally, two other *TAT* genes and *aldehyde oxidase 1* (*AO1*) were induced by Sb exposure. The expression of *S-norcoclaurine synthase* (*NCS*), a key enzyme for (S)-norcoclaurine and (S)-norlaudanosoline biosynthesis, showed concentration-dependent dynamics: up-regulated at low

Sb (Sb1) but progressively down-regulated at higher concentrations (Sb10 and Sb50) (Fig. S6A; Table S11).

Unexpectedly, comparative omics analysis uncovered a non-overlapping regulatory patterns between DEGs (Fig. S6A) and DAMs (Fig. S6B) in the isoquinoline alkaloid biosynthesis pathway. While dihydrosanguinarine levels increased progressively with Sb exposure (2.06-fold higher at Sb50), corydaline decreased (3.05-fold lower at Sb50). Meanwhile, 3,4-dihydroxybenzaldehyde and protocatechualdehyde were only induced at low Sb concentrations. This observed discrepancy between transcriptional and metabolic responses may arise from: (i) limitations in metabolite detection sensitivity, (ii) post-translational regulation, or (iii) stringent analytical thresholds. Critically, the enrichment of multiple DEGs and DAMs in the isoquinoline alkaloid biosynthetic pathway strongly supports its role in soybean Sb detoxification and tolerance.

Validation of transcriptomic data by qRT-PCR

To validate the reliability of our transcriptomic data, six hub genes (*RBOHC*, *TDIF*, *CHI4*, *PER52*, *ephA*, and *HSP26-A*) identified from the WGCNA regulatory network, along with one gene each from the flavonoid biosynthesis (*PAL1*), alanine, aspartate, glutamate metabolism (*GS1*), and isoquinoline alkaloid biosynthesis (*NCS2*) pathways, were selected for qRT-PCR verification (The primers are detailed in Table S12). Comparative analysis of RNA-Seq (Fig. 7A) and qRT-PCR (Fig. 7B) data revealed that eight of the nine tested genes showed concentration-dependent upregulation under Sb treatment (Sb1, Sb10, and Sb50), while only *NCS2* showed significant downregulation specifically under Sb50 treatment. Correlation analysis demonstrated strong consistency (R^2 = 0.799) between qRT-PCR results and RNA-Seq data across different Sb treatments (Fig. 7C). These findings robustly confirm the reliability of our transcriptomic data for subsequent analyses.

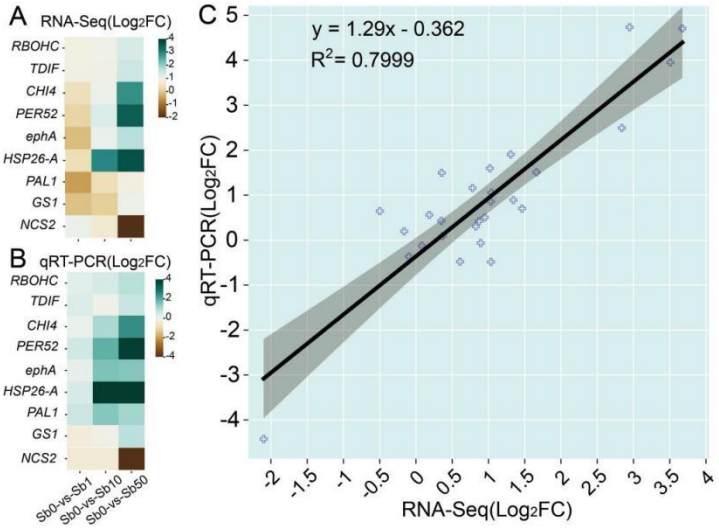

Figure 7. Validation of transcriptomic data by qRT-PCR. A. RNA-Seq expression heatmap of nine selected genes. **B** qRT-PCR validation heatmap of nine selected genes. **C** Collinearity analysis of nine representative gene RNA-Seq and qRT-PCR validation data under different Sb treatment conditions.

Discussion

Sb, an environmentally pervasive yet frequently overlooked metalloid,has gained increasing research attention due to its extensive industrial use and recognized carcinogenic potential [4]. Maintaining soybean productivity is essential for global food and edible oil security. While HMs tolerance in soybean has been well characterized for elements such as lead (Pb) [26], cadmium (Cd) [27], mercury (Hg) [28], and manganese (Mn) [29], the mechanisms underlying Sb tolerance remain poorly understood. This study systematically examines Sb accumulation, physiological stress responses, and multi-omics (transcriptomic and metabolomic) regulation in soybean under gradient Sb stress, providing a molecular foundation for breeding Sb-resistant cultivars suitable for contaminated agricultural environments.

Effects of Sb toxicity on plant growth and physiological responses

Sb toxicity has been widely documented to inhibit plant growth and development [9,10,12]. In soybean seedlings, responses varied with soil Sb concentration: high-level Sb50 (424.0 mg/kg) induced leaf wilting, whereas low-level Sb1 (10.8 mg/kg) impaired root epidermal integrity and suppressed shoot growth. Similar effects were observed in Sb-tolerant tall fescue (*Festuca arundinacea*), where 200 mg/L Sb significantly reduced root/shoot biomass and growth rates, despite its tolerance to 20 mg/L [14]. Soybean also demonstrated a strong capacity for Sb accumulation, with bioconcentration factors (BCFs > 1) and translocation factors (TFs > 0.91 for roots, stems, and leaves) (Table S2), indicating tissue Sb levels were closely correlated with soil concentrations. These findings align with previous findings of substantial Sb(III) and Sb(V) accumulation (BCFs >5) in soybean, notably including the high translocation efficiency from stems to leaves [30]. Given the efficient root-to-shoot translocation shown here, Sb accumulation in edible seeds may pose a food safety risk in contaminated areas, a possibility that should be evaluated in future studies.

In *Brassica napus*, Sb exposure (≤ 75 mg/L) activated antioxidant defenses (SOD, POD, CAT) and increased MDA levels, defining a tolerance threshold [31]. Similarly, soybean roots under high Sb50 stress (424.0 mg/kg) stress exhibited significant oxidative stress, reflected by increased CAT, SOD, MDA, and GSH levels. At Sb10 (90.0 mg/kg), despite the absence of visible leaf symptoms or biomass reduction, decreased SOD activity and GSH content relative to the control indicated that soybean tolerance was maintained within this range. Photosynthetic function was notably impaired under Sb stress, as shown by reduced chlorophyll content, consistent with reports in *Acorus calamus* [9], where Sb diminished pigment levels and suppressed photosynthetic capacity. Correspondingly, Sb stress has been shown to downregulate photosynthesis -related gene expression in *B. napu*s leaves [31]. These collective findings suggest that Sb toxicity primarily disrupts photosynthesis by interfering with pigment biosynthesis and related metabolic pathways.

Identification of key Sb-responsive genes in soybean

Plants possess diverse plasma membrane transporters that mediate HMs uptake, sequestration, and ion homeostasis maintenance, including zinc-iron permeases (ZIPs), ATP-binding cassette (ABC) transporters, heavy metal ATPases (HMAs), and metal tolerance proteins (MTPs) [32]. Relevant evidence indicates that following HM absorption and translocation, specific ABC transporter subfamilies facilitate vacuolar sequestration. For instance, Cd-tolerant rapeseed cultivars show enhanced Cd accumulation in stem vacuoles and root pectin compared to sensitive varieties,

with *BnaCn.ABCC3* identified as a key candidate gene for Cd transport [33]. In this study, transcriptomic and metabolomic analyses revealed significant enrichment of the ABC transporter pathway (ko02010) among both DEGs (Fig. 3C) and DAMs (Fig. 5D), with 18 genes (including *ABCB11*, *ABCC3*, and *ABCG20*) exhibiting upregulated expression under Sb stress. Future work should quantify Sb accumulation in subcellular compartments such as vacuoles to clarify its relationship with ABC transporter activity.

The cytochrome P450s (CYPs) superfamily, a class of heme-thiolate oxidoreductases, plays pivotal roles in biosynthetic pathways and xenobiotic detoxification, encompassing carbon source assimilation, detoxification, and secondary metabolite production. CYP-mediated detoxification involves phytohormone signaling pathways that help mitigate abiotic stresses (e.g., drought, heat, salinity, and HM toxicity) [34]. For example, the *CYP88A* participates in gibberellin biosynthesis in maize, coordinating cross-hormonal signaling to alleviate aluminum toxicity stress [35]. In soybean, genes from the *CYP71*, *CYP75*, *CYP81*, and *CYP93* families were upregulated in a dose -dependent manner under Sb stress. Their expression coincided with changes in DEGs related to terpenoid, flavonoid, alkaloid, and phenylpropanoid biosynthesis, suggesting that these metabolic pathways are likely regulated by *CYPs* [34]. These findings support the view that *CYPs* contribute to Sb detoxification through the coordinated modulation of secondary metabolites and phytohormones.

Multiple *HSP26-A* (*GSTU23*) genes were identified as potentially involved in Sb absorption and detoxification. Glutathione S-transferases (GSTs) are known for their roles in cellular detoxification and plant development. Consistent with previous reports of enhanced salt stress tolerance in poplar through *GSTU23* and *GSTU40* overexpression [36], the conserved function of *GmGSTU23* in soybean has been confirmed [37], strongly supporting its role in Sb detoxification. This evolutionary conservation strongly implicates *GmGSTU23* in Sb detoxification. Additionally, other defense-related genes, including *RBOHC*, *PER52*, and *CHI4*, were implicated in the Sb stress response network, highlighting the multi-gene regulatory framework underlying soybean adaptation to Sb toxicity.

Flavonoid Biosynthesis as a Key Pathway in Soybean Tolerance to Sb Stress

Common flavonoid compounds, including flavones, flavonols, anthocyanidins, and chalcones, are widely distributed in plant tissues and play dual roles in growth regulation and ROS detoxification under various stresses such as UV-B, chilling, salinity, drought, and HMs exposure [20, 38, 39]. HMs stress induces the generation of cytotoxic ROS including superoxide radicals (O_2^-), hydroxyl radicals (OH), and hydrogen peroxide (H_2O_2), resulting in lipid peroxidation and oxidative damage [39, 40]. In this study, elevated activities of CAT and SOD, together with increased MDA and GSH levels under high Sb treatment, confirmed the occurrence of Sb-induced oxidative stress in soybean. Notably, key genes involved in flavonoid biosynthesis (*PAL*, *4CL*, *CHS*, and *CHI*) were upregulated under Sb stress, accompanied by the accumulation of flavonoid metabolites such as isoliquiritigenin, butein, liquiritigenin, and naringenin chalcone (Fig. 6A). These results are consistent with previous studies in *Sedum plumbizincicola* [41], *Citrus grandis* [42], and *Festuca arundinacea* [43], where enhanced HMs tolerance was attributed to flavonoid-mediated metal chelation and ROS scavenging. Heavy metal stress is known to activate phenylalanine ammonia-lyase (PAL), the key enzyme initiating the phenylpropanoid pathway, which converts L-phenylalanine to cinnamic acid and promotes flavonoid

biosynthesis [44]. Notably, PAL has been implicated in Cd stress responses, while *4CL* and *CYP* genes have been identified as crucial for Sb detoxification in tall fescue [43, 45]. Our integrated transcriptomic and metabolomic analyses establish a pivotal role for flavonoid biosynthesis in soybean Sb tolerance, suggesting that *PAL*, *4CL*, *CHS*, and *CHI* collectively facilitate the production of key flavonoid intermediates that alleviate Sb toxicity via metal chelation and antioxidant activity.

Furthermore, in conjunction with previous reports [21-25, 43], this study provides new evidence that alanine, aspartate, and glutamate metabolism, together with isoquinoline alkaloid biosynthesis, constitute additional key mechanisms in soybean Sb tolerance. These pathways form an integrated metabolic network that coordinates heavy metal detoxification in plants.

Conclusions

Gradient exposure experiments demonstrated that high-concentration Sb treatment induced significant phytotoxicity in soybean seedlings, manifested as leaf wilting, root membrane damage, and reduced biomass, while the plants also exhibited considerable Sb tolerance, accumulation, and translocation capacity. Physiological analyses confirmed Sb-induced oxidative stress, underscoring its strong physiological toxicity. Integrated multi-omics analysis revealed that the numbers of DEGs and DAMs increased in a concentration-dependent manner. This was accompanied by the progressive upregulation of key detoxification components, including ABC transporters, the CYP superfamily, and *HSP26-A* genes. Notably, flavonoid biosynthesis, alanine, aspartate and glutamate metabolism, and isoquinoline alkaloid biosynthesis pathways were identified as likely key mechanisms in Sb detoxification, collectively forming a sophisticated defense network against Sb toxicity.

Abbreviations

The following abbreviations are used in this manuscript:

Sb	Antimony
Mn	Manganese
Hg	Mercury
Pb	Lead
Cd	Cadmium
Se	Selenium
USEPA	The US Environmental Protection Agency
EU	European Union
SOD	Superoxide Dismutase
CAT	Catalase
APX	Ascorbate Peroxidase
POD	Peroxidase
MDA	Malondialdehyde
GSH	Glutathione
DEGs	Differentially Expressed Genes
DAMs	Differentially Accumulated Metabolites
POS	Positive Ion Mode

NEG	Negative Ion Mode
OPLS-DA	Orthogonal Partial Least Squares Discriminant Analysis
VIP	Variable Importance on Projection
qRT-PCR	Quantitative Real-time PCR
BCFs	Bioconcentration Factors
TFs	Translocation Factors
ZIPs	Zinc-iron Permeases
MTP	Metal Tolerance Protein
ABC	ATP-binding Cassette Transporter
HMAs	Heavy Metal ATPases
WGCNA	Weighted Gene Co-expression Network Analysis
GO	Gene Ontology
KEGG	Kyoto Encyclopedia of Genes and Genomes
FPKM	Fragments per Kilobase of Transcript per Million Fragments Mapped
ROS	Reactive Oxygen Species

Acknowledgements

Author Contributions

LY, SG, GJ, YWC and XW performed experiments, collected samples, and collected data. LY, SG, RD, YY, YC and XL analyzed the data, wrote the manuscript, and edited and revised the manuscript. JH, GX and YC examination and supervision. LY, YY and XL designed the experiment, applied for funds to support this research, and reviewed the manuscript. All authors contributed to the article and approved the submitted version.

Funding

This research was supported by Research Foundation of Education Bureau of Hunan Province, China (23B0809), the Natural Science Foundation of Hunan Province (2025JJ70318, 2023JJ50083), the National Natural Science Foundation of China (32371589) and the construct program of plant protection applied characteristic discipline in Hunan Province.

Data Availability Statement

The transcriptome sequencing data generated in this study have been deposited in the China National Center for Bioinformation (CNCB, https://www.cncb.ac.cn/) under BioProject accession number PRJCA051199.

Declarations

Ethics approval and consent to participate

The commercial soybean cultivar ‘Zhonghuang 13’, provided by the Crop Research Institute of the Hunan Academy of Agricultural Sciences, was used in this study. The collection of plant materials complied with relevant institutional, national, and international guidelines and legislation.

Consent for publication

Not applicable.

Competing interests

The authors declare no competing interests.

Author details

[1] College of Agriculture and biology, Hunan University of Humanities, Science and Technology, Key Laboratory of Development and Utilization and Quality and Safety Control of Characteristic Agricultural Resources in Central Hunan of College of Hunan Province, Loudi, Hunan 417000, China.
[2] Loudi Institute of Agricultural Sciences, Loudi 417000, China
[3] College of Agronomy, Hunan Agricultural University, Changsha, Hunan 410128, China
[4] Crop Research Institute, Hunan Academy of Agricultural Sciences, Changsha, 410125, China
[5] Yuelushan Laboratory, Changsha, 410128, China
† These authors contributed equally to this work.
* Correspondence: xjliu82@126.com

References

1. Riyazuddin R, Nisha N, Ejaz B, Khan MIR, Kumar M, Ramteke PW, et al. A Comprehensive Review on the Heavy Metal Toxicity and Sequestration in Plants. Biomolecules. 2021; 12(1): 43.
2. Bolan N, Kumar M, Singh E, Kumar A, Singh L, Kumar S, et al. Antimony contamination and its risk management in complex environmental settings: A review. Environ Int. 2022; 158:106908.
3. Dupont D, Arnout S, Jones PT, Binnemans K. Antimony Recovery from End-of-Life Products and Industrial Process Residues: A Critical Review. Journal of Sustainable Metallurgy. 2016; 2(1):79-103.
4. Fu X, Xie X, Charlet LH, Jing. A review on distribution, biogeochemistry of antimony in water and its environmental risk. J Hydrol. 2023; 625: 130043.
5. Safeer R, Liu G, Yousaf B, Ashraf A, Haider MIS, Cheema AI, et al. Insights into the biogeochemical transformation, environmental impacts and biochar-based soil decontamination of antimony. Environ Res. 2024; 251:118645.
6. Mitsunobu S, Harada T, Takahashi Y. Comparison of antimony behavior with that of arsenic under various soil redox conditions. Environ Sci Technol. 2006; 40(23):7270-7276.
7. Wu Z, Jiang Q, Yan T, Xu S, Shi H, Peng L, et al. Antimony symplastic and apoplastic absorption, compartmentation, and xylem translocation in *Brassica parachinensis* L. under antimonate and antimonite. Ecotoxicol Environ Saf. 2020; 197:110621.
8. Dong Z, He M, Lin C, Ouyang W, Liu X. Uptake, accumulation and gene response of Sb(V) in *Arabidopsis thaliana*. Ecotoxicol Environ Saf. 2024; 288:117371.
9. Zhou X, Sun C, Zhu P, Liu F. Effects of antimony stress on photosynthesis and growth of *Acorus calamus*. Front Plant Sci. 2018; 9:579.
10. Zhu Y, Li Z, Shen J, Wu K, Zhao P, Wu Z, et al. Toxicity of different forms of antimony to rice plants: Photosynthetic electron transfer, gas exchange, photosynthetic efficiency, and carbon assimilation combined with metabolome analysis. J Hazard Mater. 2022; 437:129433.
11. Feng R, Lei L, Su J, Zhang R, Zhu Y, Chen W, et al. Toxicity of different forms of antimony to rice plant: Effects on root exudates, cell wall components, endogenous hormones and antioxidant system. Sci Total Environ. 2020; 711:134589.
12. Tang H, Meng G, Xiang J, Mahmood A, Xiang G, SanaUllah, et al. Toxic effects of antimony in plants: Reasons and remediation possibilities-A review and future prospects. Front Plant Sci. 2022; 13:1011945.
13. Zhao P, Wu Z, Zheng Y, Shen J, Zhu Y, Chen Q, et al. Selenite affected photosynthesis of *Oryza sativa* L. exposed to antimonite: Electron transfer, carbon fixation, pigment synthesis via a combined analysis of physiology and transcriptome. Plant Physiol Biochem. 2023; 201:107904.
14. Fan J, Chen Y, Li X, Huang J, Zhang X, Chen K, et al. Transcriptomic and metabolomic insights into the antimony stress response of tall fescue (*Festuca arundinacea*). Sci Total Environ. 2024; 933:172990.
15. Lu Y, Peng F, Wang Y, Yang Z, Li H. Transcriptomic analysis reveals the molecular mechanisms of *Boehmeria nivea* L. in response to antimonite and antimonate stresses. J Environ Manage. 2023; 343:118195.

16. Ko KP, Park SK, Yang JJ, Ma SH, Gwack J, Shin A, et al. Intake of soy products and other foods and gastric cancer risk: a prospective study. J Epidemiol. 2013; 23(5):337-343.
17. Xu L, Chen X, Wang Q, Zhao M, Qiao Y, Xie Z, et al. Metabolomic and transcriptomic analysis revealed the maturation mechanism of White-Fleshed Strawberry. Agronomy. 2024; 14(12):2860.
18. You L, Sheng J, Jiang G, Chen H, Yuan Y, Gong S, et al. Molecular characterization and expression patterns of MTP genes under heavy metal stress in mustard (*Brassica juncea* L.). Sci Rep. 2024; 14(1):17857.
19. Wang L, Ding X, Gao Y, Yang S. Genome-wide identification and characterization of *GRAS* genes in soybean (*Glycine max*). BMC Plant Biol. 2020; 20(1):415.
20. Shomali A, Das S, Arif N, Sarraf M, Zahra N, Yadav V, et al. Diverse physiological roles of flavonoids in plant environmental stress responses and tolerance. Plants (Basel). 2022; 11(22): 3158.
21. Saeed W, Mubeen S, Pan J, Rehman M, Fang W, Luo D, et al. Integrated physiological and metabolomic responses reveal mechanisms of Cd tolerance and detoxification in kenaf (*Hibiscus cannabinus* L.) under Cd stress. Front Plant Sci. 2024; 15:1332426.
22. Liu T, Zhang K, Ming C, Tian J, Teng H, Xu Z, et al. Lead toxicity in *Nicotiana tabacum* L.: Damage antioxidant system and disturb plant metabolism. Ecotoxicol Environ Saf. 2025; 291:117837.
23. Liu Y, Zheng J, Ge L, Tang H, Hu J, Li X, et al. Integrated metabolomic and transcriptomic analyses reveal the roles of alanine, aspartate and glutamate metabolism and glutathione metabolism in response to salt stress in tomato. Sci Hortic-Amsterdam. 2024; 328:112911.
24. Mondal A, Gandhi A, Fimognari C, Atanasov AG, Bishayee A. Alkaloids for cancer prevention and therapy: Current progress and future perspectives. Eur J Pharmacol. 2019; 858:172472.
25. Li L, Yan X, Li J, Wu X, Wang X. Metabolome and transcriptome association analysis revealed key factors involved in melatonin mediated cadmium-stress tolerance in cotton. Front Plant Sci. 2022; 13:995205.
26. Vergara Cid C, Pignata ML, Rodriguez JH. Effects of co-cropping on soybean growth and stress response in lead-polluted soils. Chemosphere. 2020; 246:125833.
27. Wang P, Deng X, Huang Y, Fang X, Zhang J, Wan H, et al. Root morphological responses of five soybean [*Glycine max* (L.) Merr] cultivars to cadmium stress at young seedlings. Environ Sci Pollut Res Int. 2016; 23(2):1860-1872.
28. Chen J, Yang ZM. Mercury toxicity, molecular response and tolerance in higher plants. Biometals. 2012; 25(5):847-857.
29. Santos EF, Kondo Santini JM, Paixão AP, Júnior EF, Lavres J, Campos M, et al. Physiological highlights of manganese toxicity symptoms in soybean plants: Mn toxicity responses. Plant Physiol Biochem. 2017; 113:6-19.
30. Cao W, Gong J, Zeng G, Song B, Zhang P, Li J, et al. Potential Interactions between three common metal oxide nanoparticles and Antimony(III/V) involving their uptake, distribution, and phytotoxicity to soybean. ACS Sustainable Chem Eng. 2020; 8(27):10125-10141.
31. Liu X, You L, Yu W, Yuan Y, Zhang W, Yan M, et al. Transcriptome profiles of leaves and roots of *Brassica napus* L. in response to antimony stress. Sci Rep. 2025; 15(1):9413.
32. Ghuge SA, Nikalje GC, Kadam US, Suprasanna P, Hong JC. Comprehensive mechanisms of heavy metal toxicity in plants, detoxification, and remediation. J Hazard Mater. 2023; 450:131039.
33. Zhang ZH, Zhou T, Tang TJ, Song HX, Guan CY, Huang JY, et al. A multiomics approach reveals the pivotal role of subcellular reallocation in determining rapeseed resistance to cadmium toxicity. J Exp Bot. 2019; 70(19):5437-5455.

34. Chakraborty P, Biswas A, Dey S, Bhattacharjee T, Chakrabarty S. Cytochrome P450 gene families: role in plant secondary metabolites production and plant defense. J Xenobiotics. 2023; 13(3):402-423.
35. Guo P, Bai G, Carver B, Li R, Bernardo A, Baum M. Transcriptional analysis between two wheat near-isogenic lines contrasting in aluminum tolerance under aluminum stress. Molecular genetics and genomics : MGG. 2007; 277(1):1-12.
36. Niu MX, Feng CH, Liu M, Liu X, Liu S, Liu C, et al. Genome-wide identification of poplar *GSTU* gene family and its *PtrGSTU23* and *PtrGSTU40* to improve salt tolerance in poplar. Ind Cros Prod. 2024; 209: 117945.
37. Li X, Pang Y, Zhong Y, Cai Z, Ma Q, Wen K, *et al*. *GmGSTU23* Encoding a Tau class glutathione S-Transferase protein enhances the salt tolerance of Soybean (*Glycine max* L.). Int J Mol Sci. 2023; 24(6): 5547.
38. Kumar V, Suman U, Rubal, Yadav SK. Flavonoid secondary metabolite: Biosynthesis and role in growth and development in plants. Singapore: Springer Singapore, 2018: 19-45.
39. Zhuang WB, Li YH, Shu XC, Pu YT, Wang XJ, Wang T, et al. The classification, molecular structure and biological biosynthesis of flavonoids, and their roles in biotic and abiotic stresses. Molecules. 2023; 28(8): 3599.
40. Jamla M, Khare T, Joshi S, Patil S, Kumar V. Omics approaches for understanding heavy metal responses and tolerance in plants. Curr Plant Biol. 2021; 27:100213.
41. Zhu Y, Qiu W, He X, Wu L, Bi D, Deng Z, et al. Integrative analysis of transcriptome and proteome provides insights into adaptation to cadmium stress in *Sedum plumbizincicola*. Ecotoxicol Environ Saf. 2022; 230:113149.
42. Ren Q-Q, Huang ZR, Huang WL, Huang WT, Chen H-H, Yang LT, et al. Physiological and molecular adaptations of *Citrus grandis* roots to long-term copper excess revealed by physiology, metabolome and transcriptome. Environ Exp Bot. 2022; 203:105049.
43. Li X, Wu F, Xiang Y, Fan J. Transcriptomic analysis of antimony response in Tall Fescue (*Festuca arundinacea*). Agriculture. 2024; 14(9):1504.
44. Šamec D, Karalija E, Šola I, Vujčić Bok V, Salopek-Sondi B. The role of polyphenols in abiotic stress response: The influence of molecular structure. Plants (Basel). 2021; 10(1): 118.
45. Goncharuk EA, Zagoskina NV. Heavy Metals, Their phytotoxicity, and the role of phenolic antioxidants in plant stress responses with focus on Cadmium: Review. Molecules. 2023; 28(9): 3921.

Supplementary Files

This is a list of supplementary files associated with this preprint. Click to download.

- Supplementarytable112.xlsx
- SupplementaryFigure16.docx